Current Research in Pharmacology and Drug Discovery 3 (2022) 100111

Contents lists available at ScienceDirect

Current Research in Pharmacology and Drug Discovery

journal homepage: www.journals.elsevier.com/current-research-in-pharmacology-and-drug-discovery

Three-dimensional spheroids of choroid-retinal vascular endothelial cells as an *in-vitro* model for diabetic retinopathy: Proof-of-concept investigation

Manish Gore [a,1], Ankit Tiwari [a,1], Devashree Jahagirdar [a], Angayarkanni Narayanasamy [c], Ratnesh Jain [b,**], Prajakta Dandekar [a,*]

[a] Department of Pharmaceutical Sciences and Technology, Institute of Chemical Technology, Mumbai, 400 019, India
[b] Department of Chemical Engineering, Institute of Chemical Technology, Mumbai, 400 019, India
[c] Department of Biochemistry and Cell Biology, Vision Research Foundation, Sankara Nethralaya, Chennai, 600 006, India

ARTICLE INFO

Keywords:
Diabetic retinopathy
Three-dimensional
In-vitro
Choroid-retinal vascular endothelial cells
Spheroids
Angiogenesis

ABSTRACT

Diabetic retinopathy (DR) is a primary microvascular complication of *diabetes mellitus* and a vision-threatening condition. Vascular endothelial growth factor (VEGF) induces neovascularization and causes metabolic damage to the retinal and choroidal vasculature in diabetic patients. Existing drug screening models and treatment strategies for DR need to be refined through the establishment of relevant pre-clinical models, which may enable development of effective and safe therapies. The present study discusses the development of an *in-vitro* three-dimensional (3D) spheroid model, using RF/6A choroid-retinal vascular endothelial cells, to closely mimic the *in-vivo* disease condition. Compact, reproducibly-sized, viable and proliferating RF/6A spheroids were fabricated, as confirmed by microscopy, live/dead assay, cell proliferation assay and histological staining. *In-vitro* angiogenesis was studied by evaluating individual effects of VEGF and an anti-VEGF monoclonal antibody, Bevacizumab, and their combination on cellular proliferation and 3D endothelial sprout formation. VEGF stimulated angiogenic sprouting while Bevacizumab demonstrated a dose-dependent anti-angiogenic effect, as determined from the cellular proliferation observed and extent and length of sprouting. These investigations validated the potential of RF/6A spheroids in providing an alternative-to-animal, pathophysiologically-relevant model to facilitate pre-clinical and biomedical research related to DR.

1. Introduction

Diabetic retinopathy (DR) is the frequent microvascular complication of *diabetes mellitus*, a metabolic disorder that affects around half a billion people, worldwide. DR affects nearly one-third of the diabetic patients; while one-tenth of the DR-affected, working-age adults exhibit vision-impairment (Elkjaer et al., 2020; Saeedi et al., 2019; Wong and Sabanayagam, 2020). This pathological condition occurs as early-stage, non-proliferative DR (NPDR) and an advanced-stage, proliferative DR (PDR). PDR, characterized by retinal neovascularization, exacerbates as vision-threatening diabetic macular oedema (DME) in severe cases, which is caused due to the breakdown of the blood-retinal barrier (BRB) (Bandello et al., 2017; Duh et al., 2017). DR is a complex and multifactor disorder that progresses due to hypoxia-induced upregulation and overexpression of the vascular endothelial growth factor (VEGF). VEGF stimulates angiogenesis in the retinal vascular endothelial cells, which leads to retinal neovascularization and breakdown of BRB. Additionally, DR-induced neovascularization is also observed in choroidal endothelial cells. VEGF-165, majorly involved in the development of PDR and DME, acts by binding to the VEGF receptor-1 (VEGFR-1) and VEGFR-2. The VEGFR-2 play an instrumental role in mediating the effects of VEGF in DR by activating the intracellular mitogen-activated protein kinase (MAPK) signalling pathways (Crawford et al., 2009; Duh et al., 2017; Gui et al., 2020; Semeraro et al., 2015; Wang and Lo, 2018; Whitehead et al., 2018).

Vitreoretinal surgery, laser/pan-retinal photocoagulation (PRP), intra-vitreal anti-VEGF therapy and corticosteroids are the mainstay treatment strategies for DR and DME. However, vitreoretinal surgery poses the risk of vision loss, while the laser photocoagulation often leads to scarring of ocular tissues, thereby resulting to a reduced visual acuity. Anti-VEGF agents, such as off-label Bevacizumab and FDA-approved

* Corresponding author.
** Corresponding author.
E-mail addresses: rd.jain@ictmumbai.edu.in (R. Jain), pd.jain@ictmumbai.edu.in (P. Dandekar).
[1] These authors have contributed equally to this work.

https://doi.org/10.1016/j.crphar.2022.100111
Received 19 January 2022; Received in revised form 26 April 2022; Accepted 17 May 2022

Ranibizumab, Pegaptanib and Aflibercept, although efficacious in treating PDR and DME, exhibit limitations in clinical settings due to the development of therapeutic resistance, adverse effects (like corneal scarring, vitreous/conjunctival haemorrhage, inflammation, etc.) and low patient compliance due to high costs and requirement of frequent administration. On the other hand, intra-vitreous corticosteroids are associated with the risk of developing cataract and glaucoma. This indicates an immense need to develop effective and safe therapies, which may reduce and reverse progressive visual impairment in PDR and DME (Duh et al., 2017; Sarkar and Dyawanapelly, 2021; Wang and Lo, 2018; Whitehead et al., 2018).

Animal models and *in-vitro* retinal endothelial monolayer cultures have been widely used for pre-clinical screening of drugs and formulations developed against PDR and DME. However, use of animal models in pre-clinical research is a time and cost-intensive approach and demonstrates drawbacks like ethical constraints, anatomical differences, failure to mimic advanced stages of the disease, lack of availability of reagents for molecular research, poor predictability and extrapolation to clinical data, etc., thus acting as imperfect replicas of DR in humans. (Kern et al., 2019; Lai and Lo, 2013; Olivares et al., 2017; Van Norman, 2019). Also, the existing two-dimensional (2D) *in-vitro* cultures of retinal endothelial cells do not recapitulate the quiescent phenotype, generally exhibited by the retinal endothelial cells, under *in-vivo* conditions (Han et al., 2021; Heiss et al., 2015; Lazzara et al., 2019; Moleiro et al., 2017; Rezzola et al., 2014).

The present study was thus aimed at developing an alternative-to-animal, three-dimensional (3D) *in-vitro* model of choroid-retinal vascular endothelial cells, that would closely mimic the *in-vivo* disease pathophysiology. Monkey choroid-retinal vascular endothelial cells (RF/6A cells) were chosen due to their robustness, ease of maintenance and their popularity in research related to retinal vascular diseases, particularly DR (Chan et al., 2019; Chen et al., 2021; Hsu et al., 2020; Liao et al., 2020; Mynampati et al., 2017; Wang et al., 2020). 3D endothelial spheroids exhibit an *in vivo*-like quiescent endothelial phenotype, consisting of tip cells and proliferating stalk cells, when stimulated using pro-angiogenic factors like VEGF, and exhibit angiogenesis by sprout formation (Heiss et al., 2015; Rezzola et al., 2017). Thus, owing to their ability to mimic physiological vascular structures and functions (Zucchelli et al., 2019), this investigation was focused on development of 3D spheroid-based model of RF/6A cells to conduct pharmacological investigations pertaining to DR and DME. The spheroids fabricated by the matrix-free approach, were characterized by cellular and histological assays. Furthermore, *in-vitro* angiogenic cell proliferation and 3D sprout formation in spheroids was visualised by individual and combined treatment with VEGF and Bevacizumab. A dose-dependent anti-angiogenic effect of Bevacizumab on sprouting and mean sprout length confirmed the suitability of spheroids as a pre-clinical tool for assessing newer therapeutic interventions.

2. Experimental section

2.1. Materials

Rhesus monkey (*Macaca mulatta)*-derived RF/6A choroid-retinal vascular endothelial cells, at passage 45, were generously gifted by Dr. Angayarkanni Narayanasamy (Sankara Nethralaya, India). Minimum essential medium (MEM), fetal bovine serum (FBS), antibiotic antimycotic solution, EZ Blue™ cell assay kit and DPX mountant were purchased from HiMedia Laboratories Pvt. Ltd., Mumbai, India. Dulbecco's Phosphate-Buffered Saline (DPBS), trypsin-ethylenediaminetetraacetic acid (Trypsin-EDTA), Calcein AM (LIVE/DEAD® Viability/Cytotoxicity Kit), propidium iodide and optimal cutting temperature compound (OCT) were procured from ThermoFisher Scientific, USA. Corning® Costar® ultra-low attachment (ULA) U-bottom well plates, Harris haematoxylin stain, 0.5% alcoholic solution of Eosin Y and recombinant human VEGF-165 (hVEGF-165 or VEGF-165) were purchased from Sigma Aldrich, USA. Bevacizumab (Vegfxta injection, 100 mg/4 mL) was obtained from Fresenius Kabi India Pvt. Ltd., India. Matrigel® basement membrane matrix was purchased from Corning, USA.

2.2. Methods

2.2.1. Cell culture

RF/6A cells were cultured in MEM supplemented with 10% FBS and 1% antibiotic antimycotic solution. The cells were maintained in a humidified cell culture incubator at 37 °C and in presence of 5% CO_2.

2.2.2. Development and morphology of RF/6A spheroids

Corning ULA U-bottom well plates were used for the generation of matrix-free spheroids. RF/6A cells dissociated from cell culture flask at 80% confluency using 0.1% trypsin-EDTA were counted using Countess II FL Automated Cell Counter (ThermoFisher Scientific, USA). The spheroids were optimized with respect to different cell seeding densities, such as 7000, 6000, 5000, 4000, 3000, 2000, 1000 and 500 cells per well of the ULA microplate, and culture duration of 3, 5, 7, 9 and 11 days. The morphology of spheroids was assessed by phase contrast microscopy (EVOS FL Auto imaging system, ThermoFisher Scientific, USA), which revealed the optimum seeding cell density and culture duration. The average diameter and area of spheroids developed using optimal culture conditions were determined using ImageJ Fiji, an open-source imaging software.

2.2.3. Cell proliferation assay

The cell proliferation in spheroids was evaluated by using EZ Blue™ cell assay kit. This resazurin dye reduction-based *in-vitro* cell proliferation assay was performed on spheroids developed after 3, 5, 7, 9 and 11 days of 3D culture, after plating the cells at initial seeding densities of 5000, 4000, 3000, 2000, 1000 and 500 cells per well of the ULA microplate. 10% EZ Blue™ reagent was added to the spheroids at the respective time points and the samples were incubated for 4 h in a humidified cell culture incubator, at 37 °C and in presence of 5% CO_2. Further, the absorbance was measured using a microplate reader (Synergy H1 Microplate reader, BioTek Instruments, USA) at 570 nm and 600 nm. Percent dye reduction values, indicative of cellular metabolic activity or proliferation, were calculated as per manufacturer's protocol.

2.2.4. Live/dead assay and confocal microscopy

This qualitative live/dead cell viability assay was conducted using Calcein AM (Ex/Em: 494/517 nm) and Propidium Iodide (PI) (Ex/Em: 535/617 nm) dyes. Sterile working solution of these dyes were prepared in dark by mixing 0.5 μL of Calcein AM (4 mM stock solution) and 5 μL of PI (1 mg/mL stock solution) in 1 mL of DPBS. The assay was conducted as per manufacturer's protocol and the viability and 3D orientation of spheroids developed at optimum cell culture conditions were assessed using confocal laser scanning microscope (Leica Microsystems, Germany).

2.2.5. Histological staining

The spheroids formed at optimum culture conditions were fixed using 4% paraformaldehyde (PFA) in PBS, at 25 °C, for 2.5 h, and were later stored in 30% sucrose in DPBS, at 4 °C, for overnight. Further, they were embedded in OCT, inside a disposable biopsy mold and kept at −20 °C for 10–15 min, before final storage in a deep freezer at −80 °C. OCT block was further processed using a cryostat (Leica Biosystems, Germany) and 15 μm cryosections were obtained and fixed on poly-l-lysine coated slides. The cryostat sections were subjected to histochemical analysis using standard haematoxylin and eosin (H&E) staining protocol. The sections were mounted using DPX mountant and were observed by

brightfield microscopy (EVOS FL Auto imaging system, ThermoFisher Scientific, USA).

2.2.6. In-vitro angiogenesis assays

The RF/6A spheroids and 2D cell culture controls were validated using *in-vitro* angiogenesis assay, by evaluating cell proliferation and 3D sprout formation, after treatment with VEGF, Bevacizumab, and their combination.

2.2.6.1. Cell proliferation assay: Effect of VEGF, Bevacizumab, and their combination. These studies were conducted after subjecting the RF/6A cells to overnight serum starvation before seeding them in Corning ULA plates for spheroid culture.

2.2.6.1.1. Effect of VEGF, Bevacizumab, and their combination at the cell seeding stage of 3D and 2D cultures. The RF/6A 3D and 2D cultures were treated with increasing concentrations of VEGF (10, 50, 100 and 200 ng/mL) and Bevacizumab (0.1, 1, 2 and 4 mg/mL), on day 0 of cell culture. RF/6A 3D and 2D cultures were also treated with a combination of VEGF (50 ng/mL) and increasing doses of Bevacizumab (0.1, 1, 2, 4 mg/mL), on day 0 of cell culture. Both the cell cultures were treated with the individual drugs and their combination for 3 and 5 days. Thereafter, cell proliferation was measured using EZ Blue™ assay, as stated in section 2.2.3. Percent dye reduction values were determined on days 3 and 5 of treatment, as per manufacturer's protocol.

2.2.6.1.2. Effect of VEGF, Bevacizumab, and their combination after establishment of 3D and 2D cultures. RF/6A spheroids formed on the day 3 of 3D culture and RF/6A monolayers after overnight cell attachment were used in this investigation. Day 3 spheroids and day 0 attached 2D cell cultures were treated with increasing concentrations of VEGF (10, 50, 100 and 200 ng/mL) and Bevacizumab (0.1, 1, 2 and 4 mg/mL). Additionally, day 3 spheroids and day 0 attached cell monolayers were also treated with the combination of 50 ng/mL of VEGF and increasing doses of Bevacizumab (0.1, 1, 2 and 4 mg/mL), respectively. Both the cell cultures were treated with the individual drugs and their combination for 3 days. Thereafter, cell proliferation was measured using EZ Blue™ assay, as stated in section 2.2.3. Percent dye reduction values were determined after 72 h (i.e., day 3) of treatment, as per manufacturer's protocol.

2.2.6.2. 3D sprout formation assay. Compact RF/6A spheroids were aseptically collected from ULA plate in a viable state and embedded in Matrigel®. The matrix was allowed to polymerize for 30 min, at 37 °C, in a cell culture incubator. The matrix-embedded spheroids were treated with VEGF (50 ng/mL), Bevacizumab (0.1 mg/mL and 4 mg/mL) and their combination (50 ng/mL of VEGF along with 0.1 mg/mL and 4 mg/mL of Bevacizumab, respectively). 3D sprouting, indicative of angiogenic potential, was observed after 24 h of treatment by phase contrast microscopy. The microscopic images were subjected to quantitative analysis, using the WimSprout analysis (Wimasis image analysis, Córdoba, Spain), to determine the mean and cumulative sprout lengths.

2.3. Statistical analysis

All experiments were conducted in triplicates. Data has been reported as the mean ± standard deviation (SD). In studies involving three or more treatment conditions and a single time point, statistical analysis was conducted using one-way analysis of variance (ANOVA), with multiple comparisons. On the other hand, studies involving three or more treatment conditions and more than one time points were statistically analysed using two-way ANOVA, with multiple comparisons. Statistical significance was determined by calculating P values using Tukey HSD (honest significant difference) post-hoc analysis. P value less than 0.05 ($P < 0.05$) was considered to be significant. ANOVA and Tukey HSD post-hoc tests were conducted using Prism Version 8.0.2, GraphPad software Inc., USA.

3. Results

3.1. Characterization of RF/6A spheroids

Spheroids developed using different cell seeding numbers and durations of cell culture have been represented in Supplementary Fig. 1 (Fig. S1). In addition, the outcomes of the live/dead staining and *in-vitro* cell proliferation assays, observed with different seeding densities and durations of spheroid culture, have been provided in Figs. S2 and S3. It was observed that the seeding density of 5000 cells per well resulted in the formation of compact spheroids, with desirable integrity and reproducible geometry, after 5 days of culture, as shown in Fig. 1A. Analysis by ImageJ Fiji revealed that the mean diameter and area of spheroids were 253 ± 6 μm and 50,252 ± 26 μm^2, respectively. Further, the presence and distribution of Calcein AM-stained live cells, observed as green fluorescence, and PI-stained dead cells, observed as red fluorescence, indicated a higher proportion of live cells, which ascertained the viability of spheroids at optimum culture conditions. Z-stack confocal imaging at day 5 of culture, as depicted in Fig. 1B, confirmed the viability and 3D structure of the RF/6A spheroids. Also, the microscopic image of H & E stained-section, represented in Fig. 1C, demonstrated a uniform distribution of cells within the spheroid and exhibited the presence of small luminal areas.

3.2. Cell proliferation assay: Effect of VEGF, Bevacizumab, and their combination

3.2.1. Effect of VEGF on 3D and 2D RF/6A cultures

As observed in Fig. 2A, B and 3A, treatment with VEGF did not result in significant dye reduction at the concentrations and durations evaluated during the study, both at the cell seeding stage and after the formation of spheroids. Particularly the group treated with 200 ng/mL of VEGF exhibited a slightly significant decrease ($P = 0.02$) in the mean percent dye reduction on day 5 of culture, as compared to the control. These results have been depicted in Fig. 2B. Similar effects were also observed in 2D cell cultures, as shown in Fig. S4A, S4B and S5A, when

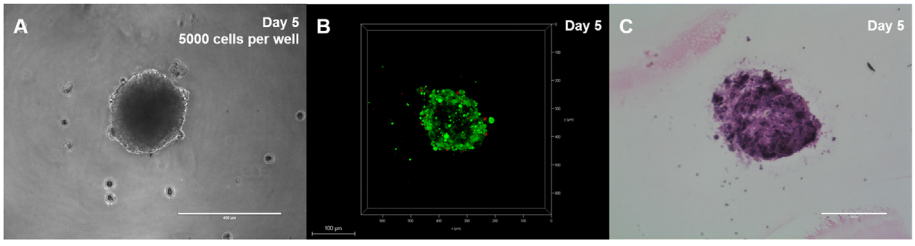

Fig. 1. Characterization of day 5 RF/6A spheroids developed using the seeding density of 5000 cells per well for cell morphology, viability, and histology. (A) Phase contrast microscopic image of RF/6A spheroid (Scale bar: 400 μm); **(B)** Z-stack confocal image representing viability and 3D orientation of the RF/6A spheroid (Scale bar: 100 μm); **(C)** Brightfield microscopic image of H&E-stained cross-section of RF/6A spheroid (Scale bar: 100 μm).

tested at the cell seeding stage and after cell attachment.

3.2.2. Effect of Bevacizumab on 3D and 2D RF/6A cultures

Fig. 2C and D demonstrate the day 3 and day 5 effects of Bevacizumab, after treatment at the cell seeding stage of 3D culture. Dose-dependent, statistically significant decrease in the mean percent dye reduction was observed on day 3 (Fig. 2C) in the groups treated with 2 mg/mL ($P = 0.0022$) and 4 mg/mL ($P < 0.0001$) of Bevacizumab, as compared to the control. Similar effect was observed in the groups treated with Bevacizumab, at all the test doses, on day 5 of 3D culture (Fig. 2D), as compared to the control. Here, P values were found to be 0.0078 in case of the group treated with 0.1 mg/mL of Bevacizumab and <0.0001 with the other doses. Results of treating 2D cultures with Bevacizumab at the cell seeding stage have been demonstrated in Figs. S4C and S4D, for days 3 and 5 of cell culture, respectively. The average percent dye reduction observed on days 3 and 5 revealed a dose-dependent decrease in cell proliferation, as compared to the respective controls. The effects observed on day 3 of cell culture (Fig. S4C) were significant for groups treated with 1 mg/mL ($P = 0.0033$), 2 mg/mL ($P = 0.0001$) and 4 mg/mL ($P < 0.0001$) of Bevacizumab, as compared to the control group. Significant effects for day 5 (Fig. S4D) were observed for the groups treated with 1 mg/mL ($P = 0.04$), 2 mg/mL and 4 mg/mL ($P < 0.0001$) of Bevacizumab, relative to the control group.

Besides this, as observed in Fig. 3B, treatment with 4 mg/mL of Bevacizumab ($P = 0.01$) for 3 days resulted in a slightly significant decrease in mean percent dye reduction in the group treated after spheroid formation, while effects at other doses were non-significant. On the other hand, as observed on day 3 of the treatment, Bevacizumab did not result in significant dye reduction in the attached 2D cultures at the doses tested during this study (Fig. S5B).

3.2.3. Effect of the combination of VEGF and Bevacizumab on 3D and 2D RF/6A cultures

Fig. 2E and F depict the day 3 and day 5 effects of combination of VEGF and Bevacizumab, observed after treatment at the cell seeding stage of 3D culture. Combined treatment resulted in a dose-dependent decrease in the mean percent dye reduction, wherein a significant effect (Fig. 2E) was observed on day 3 for the group treated with a combination of 50 ng/mL of VEGF and 4 mg/mL of Bevacizumab ($P = 0.0001$). Similar findings were observed on day 5 of culture (Fig. 2F), wherein the significant effects were recorded for all the combinations comprising of 50 ng/mL of VEGF and 0.1 mg/mL ($P = 0.0066$), 1 mg/mL ($P = 0.0025$), 2 mg/mL and 4 mg/mL ($P < 0.0001$) of Bevacizumab, as compared to the control group.

Outcomes of treatment with combination of VEGF and Bevacizumab at the cell seeding stage of 2D culture have been demonstrated in Figs. S4E and S4F, as observed on days 3 and 5 of cell culture, respectively. Dose-dependent decrease in the average percent dye reduction was found to be significant on day 3 (Fig. S4E) for the combination group treated with 50 ng/mL of VEGF and 4 mg/mL of Bevacizumab ($P < 0.0001$), as compared to the control. Similar outcomes were observed on day 5 of treatment (Fig. S4F), wherein significant results were observed upon treatment with 50 ng/mL of VEGF and 1 mg/mL ($P = 0.01$), 2 mg/mL ($P = 0.0048$) and 4 mg/mL ($P < 0.0001$) of Bevacizumab, respectively, relative to the control.

Effect of the combination of VEGF (50 ng/mL) and different doses of Bevacizumab on well-formed RF/6A spheroids has been depicted in Fig. 3C. A dose-dependent decrease in the mean percent dye reduction values was observed for all groups treated with the drug combination for 3 days, relative to the control. This effect was significant in spheroids treated with 50 ng/mL of VEGF and 0.1 mg/mL ($P = 0.0003$), 1 mg/mL ($P = 0.0002$), 2 mg/mL and 4 mg/mL ($P < 0.0001$) of Bevacizumab, respectively.

Furthermore, results of treatment with the combination of VEGF (50 ng/mL) and different doses of Bevacizumab, after 3 days of attachment of RF/6A monolayers, have been depicted in Fig. S5C. In this group, a dose-dependent significant decrease in the mean dye reduction was noted for the group treated with 50 ng/mL of VEGF and 4 mg/mL of Bevacizumab ($P = 0.0051$).

Comparison of day 3 and day 5 effects of treatment with VEGF, Bevacizumab, and their combination at the cell seeding stage of 3D and 2D cell cultures were also studied and have been summarized in Fig. S6.

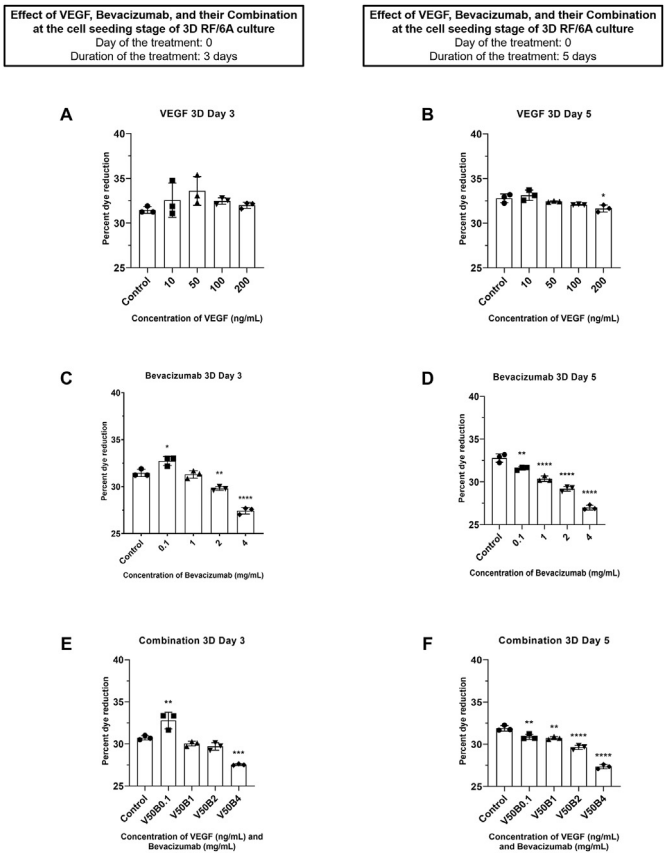

Fig. 2. Results of resazurin dye reduction-based *in-vitro* cell proliferation assay observed after treating the 3D RF/6A culture with VEGF, Bevacizumab, and their combination at the cell seeding stage (day 0) for 3 days (Fig. 2A, C, E) and 5 days (Fig. 2B, D, F), respectively. Percent dye reduction has been represented as mean ± SD. Results of one-way ANOVA analysis were considered significant at P values less than 0.05 ($P < 0.05$). Statistical significance in day 3 and day 5 results were determined relative to the respective controls. **(A)** Effect of VEGF (10–200 ng/mL) on day 3 relative to the control; **(B)** Effect of VEGF (10–200 ng/mL) on day 5 relative to the control; **(C)** Effect of Bevacizumab (0.1–4 mg/mL) on day 3 relative to the control; **(D)** Effect of Bevacizumab (0.1–4 mg/L) on day 5 relative to the control; **(E)** Effect of the combination of VEGF (50 ng/mL) and Bevacizumab (0.1–4 mg/mL) on day 3 relative to the control; **(F)** Effect of the combination of VEGF (50 ng/mL) and Bevacizumab (0.1–4 mg/mL) on day 5 relative to the control.

3.3. 3D Sprout formation assay: Effect of VEGF, Bevacizumab, and their combination

Results of the sprouting assay have been depicted in Fig. 4. Phase contrast images (Fig. 4A) captured after 24 h of treatment demonstrate the outcomes observed after treating Matrigel®-embedded spheroids with 50 ng/mL VEGF, 0.1 mg/mL of Bevacizumab, 4 mg/mL of Bevacizumab and the combination of 50 ng/mL of VEGF with 0.1 mg/mL or 4 mg/mL of Bevacizumab, respectively. The qualitative outcomes of WimSprout analysis obtained for control and treatment groups have been depicted in Fig. 4B. Here, the red colour indicates the skeleton of the endothelial sprouts, yellow shows the sprout number, blue demonstrates the structure of the sprouts, white indicates the end processes of the

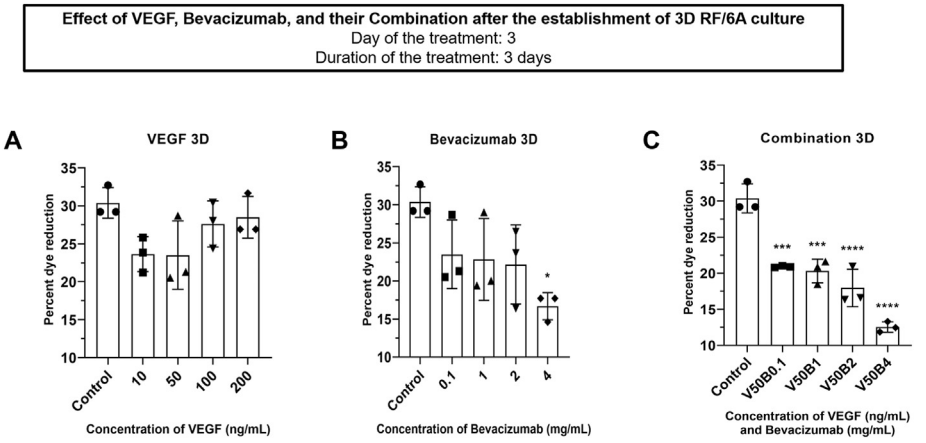

Fig. 3. Results of resazurin dye reduction-based *in-vitro* cell proliferation assay observed after treating the day 3 RF/6A spheroid culture with VEGF, Bevacizumab, and their combination for 3 days. Percent dye reduction has been represented as mean ± SD. Results of one-way ANOVA analysis were considered significant if P values were found to be less than 0.05 ($P < 0.05$). Statistical significance was determined relative to the control. **(A)** Effect of VEGF (10–200 ng/mL) relative to the control; **(B)** Effect of Bevacizumab (0.1–4 mg/mL) relative to the control; **(C)** Effect of the combination of VEGF (50 ng/mL) and Bevacizumab (0.1–4 mg/mL) relative to the control.

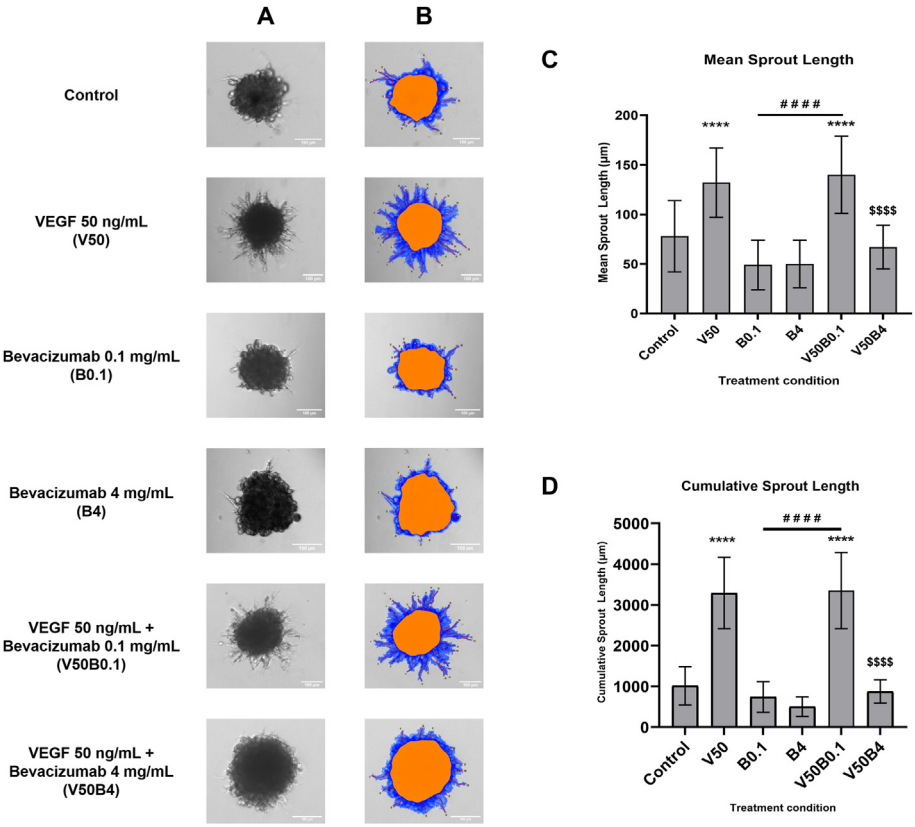

Fig. 4. Results of the 3D sprouting angiogenesis assay for RF/6A spheroid culture. (A) Phase contrast images of sprout outgrowths from Matrigel®-embedded spheroids subjected to 24 h of treatment with VEGF (50 ng/mL), Bevacizumab (0.1 mg/mL and 4 mg/mL) and their combination (Scale bar: 100 μm); **(B)** Output images of Wimsprout analysis (Scale bar: 100 μm) corresponding to the respective phase contrast images (depicted in Fig. 4A); **(C)** Mean sprout length of the Matrigel®-embedded RF/6A spheroids subjected to different treatment conditions; **(D)** Cumulative sprout length of the Matrigel®-embedded RF/6A spheroids subjected to different treatment conditions. Results of one-way ANOVA analysis for the determination of mean and cumulative sprout lengths were considered significant if the P values were found to be less than 0.05 ($P < 0.05$). Statistical significance of the treatment groups was determined relative to the control. Fig. 4C and D have been represented based on the data obtained from phase contrast microscopy images (Fig. 4A) and output images of the Wimsprout analysis (Fig. 4B).

sprouts, while the orange colour shows the structure of RF/6A spheroid.

As observed in Fig. 4A and B, the groups treated with VEGF (50 ng/mL) (i.e., V50) and the combination of 50 ng/mL of VEGF and 0.1 mg/mL of Bevacizumab (i.e., V50B0.1) resulted in higher sprouting, as compared to the respective controls. Since sprouting observed in V50 and V50B0.1-treated groups were almost similar, 0.1 mg/mL of Bevacizumab was not observed to generate any potent anti-angiogenic response in presence of VEGF. However, the extent of sprouting decreased in the spheroids treated with 0.1 mg/mL and 4 mg/mL of Bevacizumab (i.e., B0.1 and B4), as well as in the groups treated with the combination of 50 ng/mL of VEGF and 4 mg/mL of Bevacizumab (i.e., V50B4), relative to the respective controls.

Fig. 4C and D demonstrate the quantitative results of the sprouting assay, in terms of mean sprout and cumulative sprout lengths, respectively. The mean and cumulative sprout lengths were higher and statistically significant for V50 and V50B0.1 treatment groups ($P < 0.0001$), as compared to the respective controls. Statistically significant differences (denoted by '$') were observed between V50 and V50B4 treatment groups ($P < 0.0001$). Similar effects were observed upon statistical comparison (indicated by '#') between B0.1 and V50B0.1-treated groups ($P < 0.0001$). As a result, analogous to microscopic observations (Fig. 4A and B), higher sprouting was observed upon treating native spheroids with 50 ng/mL of VEGF, with and without 0.1 mg/mL of Bevacizumab. Thus, 0.1 mg/mL of Bevacizumab did not affect the sprouting in spheroids, in presence of VEGF, as also determined quantitatively. However, the sprouting was largely inhibited by treating the spheroids with 0.1 mg/mL and 4 mg/mL of Bevacizumab, as well as the combination containing 4 mg/mL of Bevacizumab, thereby, indicating

that the monoclonal antibody generated a potent anti-angiogenic response at both the test concentrations. Thus, VEGF stimulated, whereas Bevacizumab (0.1 mg/mL and 4 mg/mL) inhibited sprouting in RF/6A spheroid model. Additionally, a relatively higher concentration of Bevacizumab (i.e., 4 mg/mL) demonstrated a stronger anti-angiogenic response by inhibiting 3D sprouting, even in presence of VEGF.

4. Discussion

The size and compactness of a spheroid is governed by the cell type and its growth kinetics, composition of the culture medium, cell seeding density and duration of the culture (Leung et al., 2015; Pereira et al., 2017). Also, the growth of spheroids is reflected by their average area and diameter (Amaral et al., 2017). Thus, as explained in section 3.1, characterization studies confirmed the formation of compact, uniformly-sized, viable and proliferating 3D RF/6A spheroids at an optimized cell seeding number and duration of culture. Additionally, histological characterization successfully demonstrated the formation of solid tissue-like mass, which was not observed by conventional microscopy.

As described in section 2.2.6.1, *in-vitro* cell proliferation was studied to evaluate the effects of VEGF and Bevacizumab, both alone and in combination, at the cell-seeding stage and after the formation of 3D spheroids.

We anticipate that the non-significant results observed in the 3D culture groups, treated with VEGF at the cell seeding stage (refer to section 3.2.1), are due to the density and distribution of VEGFR-2 on RF/6A cell surface and the dissociation constant (K_d) of the receptor (Stefanini et al., 2009). On the other hand, we anticipate that the diffusional mass transport limitations posed by the compact and growing 3D structure may have led to non-significant effects of VEGF in the groups treated after spheroid formation (Mehta et al., 2012).

Hence, based on the previously reported findings with RF/6A monolayer cultures (Rusovici et al., 2013), VEGF was used at the concentration of 50 ng/mL during the studies involving treatment with the combination of VEGF and Bevacizumab.

Bevacizumab is administered at a clinically relevant dose of 1.25 mg in cases of advanced DR (Gudla et al., 2018). However, effects of doses up to 2.5 mg have been assessed in animal models and human subjects (Arevalo et al., 2011; Lashay et al., 2020; Park et al., 2016). Thus, the present study investigated the effect of Bevacizumab below, at and above the clinically relevant doses, on 3D and 2D cultures of RF/6A cells.

Overall, as described in sections 3.2.2 and 3.2.3, Bevacizumab, when tested alone as well as in the combination of VEGF, demonstrated dose-dependent anti-proliferative effects in 3D spheroids and 2D cultures. Similar effects were previously studied in 2D cultures of pig choroidal endothelial cells, RF/6A cells, bovine corneal endothelial cells, immortalized bovine retinal endothelial cells, human retinal endothelial cells, etc. (Deissler et al., 2012; Mynampati et al., 2017; Peters et al., 2007; Rusovici et al., 2011, 2013; Spitzer et al., 2006) We anticipate this effect of Bevacizumab, in combination with VEGF, to occur due to the stabilization of the G0/G1 phase of the cell cycle and inhibition of the G2/M phase, as reported earlier by Rusovici R., et al. in RF/6A monolayer culture (Rusovici et al., 2013).

Moreover, a marked reduction in the mean percent dye reduction was observed in well-formed RF/6A spheroids treated with Bevacizumab, both alone and in combination with VEGF (refer to Fig. 3B and C). We project this outcome to occur due to the inhibition of VEGF-induced proliferative effects by Bevacizumab, thereby reducing cell proliferation in RF/6A spheroids. In the absence of exogenous VEGF, Bevacizumab may have blocked the proliferative effects of VEGF secreted by the endothelial cells in a paracrine/autocrine manner (Li et al., 2017; Rusovici et al., 2013). Also, the dye reduction was typically found to be lower in 3D cultures than in 2D monolayers. This is expected to occur due to the structural barriers to mass transport posed by the 3D microtissue (Mehta et al., 2012).

Additionally, the outcomes of the 3D sprout formation assay (refer to section 3.3) were similar to those from the tube formation assay in 2D RF/6A cultures, conducted by other researchers. Based on the findings reported by Jin et al. in RF/6A monolayers, we anticipate the involvement of MEK/ERK and PI3K/Akt cell signalling pathways in achieving VEGF-mediated angiogenesis in the present model (Jin et al., 2013). On the other hand, we expect that the inhibitory effect of Bevacizumab on sprout formation, when tested alone and in combination with VEGF, was observed due to its VEGF-inhibition and/or anti-angiogenic properties. A study reported earlier by Yu Z. et al. supports this observation, wherein Bevacizumab inhibited high glucose- and VEGF-induced tube formation in RF/6A monolayer cultures (Xu et al., 2010; Yu et al., 2016).

As a result, sprouting assay enabled us to study the angiogenesis in RF/6A spheroids as well as provided understanding of the effect of pharmacological treatments in 3D model. Based on qualitative data, RF/6A cells were observed to degrade and invade into the surrounding ECM matrix in presence of VEGF. As a result, sprouting was initiated in the endothelial spheroids, wherein each sprout was projected to comprise of leading and migrating tip cells followed by the proliferating stalk cells. VEGF gradients thus guided the tip cell migration and regulated the proliferation of stalk cells in an ECM microenvironment. Hence, this assay closely replicated the *in-vivo* vascular angiogenic events like matrix degradation, cell migration, cell proliferation and cellular morphogenesis/sprouting, which occurred in a sequential manner. Previously, Tetzlaff et al. have demonstrated VEGF-induced angiogenic sprouting using human umbilical vein endothelial cell (HUVEC) spheroids developed by hanging drop method. In this study, HUVEC spheroids were embedded into the collagen matrix prior to studying the pro-angiogenic effect of VEGF. As a result, the outcomes of this investigation also confirmed the endothelial origin of RF/6A cells (Gerhardt, 2008; Goodwin, 2007; Moleiro et al., 2017; Tetzlaff and Fischer, 2018).

Based on the results observed, the present *in-vitro* RF/6A 3D spheroid model is expected to provide an effective tool for screening of existing and forthcoming pharmacological interventions, developed for treating vascular abnormalities of the retina, particularly, DR and DME. We believe that the outcomes of pre-clinical screening aimed at assessing cell proliferation will be more effective if the model is treated with the DR-specific drug candidates and/or formulations prior to the formation of compact spheroid. The treatment at the cell seeding stage will not involve mass transfer limitations presented by the spheroid-structure and thus closely replicate the *in-vivo* cellular perturbations that occur in DR. Moreover, the present model will enable researchers to conduct molecular and cellular investigations related to DR and DME. In summary, the spheroid model is projected to advance basic, biomedical and pre-clinical drug development research related to DR and DME.

Presently, spheroids have been developed using monkey-derived RF/6A cells as a model system. Bevacizumab has been shown to inhibit proliferation of VEGF-enriched retinal endothelial cells more effectively as compared to the choroidal endothelial cells (Mynampati et al., 2017). Thus, the choice of cell type in the future investigations will govern the outcomes of the study. Studies with human primary retinal and choroidal endothelial cultures may provide additional insights on basic and pre-clinical aspects of DR research. Moreover, prospective studies may also be conducted by testing the effect of Ranibizumab and Aflibercept on the spheroid model. Future studies should also aim at assessment of the effect of angiogenic modulators (i.e., inducers and inhibitors) on the expression of cell-specific markers and VEGFR2, cellular hypoxia and apoptosis, alterations in molecular mechanisms, etc. Ultimately, the current 3D mono-culture model of RF/6A cells may be extended by incorporating the retinal pericytes and muller cells to provide a complex recapitulation of the DR pathophysiology. As a result, the present study opens vast avenues of research related to DR and DME that are expected to help in combating these global health concerns in the years to come.

5. Conclusion

Compact matrix-free 3D RF/6A spheroids of reproducible-size showed maximum cell viability and proliferation along with uniform cellular distribution within the microtissue, as observed at optimal cell culture conditions. Importantly, the outcomes of sprout formation assay established the pathophysiological relevance of the present *in-vitro* spheroid model by recapitulating *in-vivo* VEGF-induced angiogenesis observed in DR. Moreover, Bevacizumab demonstrated anti-proliferative and anti-angiogenic effects, when tested alone and in the combination with VEGF, thereby achieving therapeutically-relevant responses in the spheroid model. We believe that the present alternative-to-animal, *in-vitro* RF/6A spheroid model will provide a reliable and an effective tool to conduct molecular investigations on DR pathophysiology as well as accelerate pre-clinical drug development research related to DR and DME.

CRediT authorship contribution statement

Manish Gore: Conceptualization, Methodology, Data curation, Writing – original draft. **Ankit Tiwari:** Methodology, Data curation, Writing – original draft. **Devashree Jahagirdar:** Methodology, Data curation, Writing – original draft. **Angayarkanni Narayanasamy:** Technical inputs with RF/6A cells. **Ratnesh Jain:** Conceptualization, Supervision. **Prajakta Dandekar:** Conceptualization, Writing – review & editing, Supervision.

Declaration of competing interest

The authors declare that they have no known competing financial interests or personal relationships that could have appeared to influence the work reported in this paper.

Acknowledgements

We acknowledge Mr. Suryakant and Dr. Nafisa Balasinor (National Institute of Research in Reproductive Health, Mumbai, India) for technical assistance with cryosectioning of spheroid samples. We also acknowledge Ms. Tejal Pant for assisting in confocal imaging of the spheroid samples. Mr. Manish Gore is grateful to Department of Science and Technology-Inspire division, Government of India (GoI) for the fellowship. Mr. Ankit Tiwari is thankful to Department of Biotechnology, GoI for the fellowship. Ms. Devashree Jahagirdar is thankful to Indian Council of Medical Research, GoI for the fellowship. Dr. Prajakta Dandekar and Dr. Ratnesh Jain extend their gratitude to University Grants Commission, GoI for financial assistance.

Appendix A. Supplementary data

Supplementary data to this article can be found online at https://doi.org/10.1016/j.crphar.2022.100111.

References

Amaral, R.L.F., Miranda, M., Marcato, P.D., Swiech, K., 2017. Comparative analysis of 3D bladder tumor spheroids obtained by forced floating and hanging drop methods for drug screening. Front. Physiol. 8, 605. https://doi.org/10.3389/fphys.2017.00605.

Arevalo, J.F., Sanchez, J.G., Lasave, A.F., Wu, L., Maia, M., Bonafonte, S., Brito, M., Alezzandrini, A.A., Restrepo, N., Berrocal, M.H., Saravia, M., Farah, M.E., Fromow-Guerra, J., Morales-Canton, V., 2011. Intravitreal bevacizumab (avastin) for diabetic retinopathy: the 2010 GLADAOF lecture. J. Ophthalmol., 584238 https://doi.org/10.1155/2011/584238.

Bandello, F., Battaglia Parodi, M., Lanzetta, P., Loewenstein, A., Massin, P., Menchini, F., Veritti, D., 2017. Diabetic macular edema. Dev. Ophthalmol. 58, 102–138. https://doi.org/10.1159/000455277.

Chan, C.M., Hsiao, C.Y., Li, H.J., Fang, J.Y., Chang, D.C., Hung, C.F., 2019. The inhibitory effects of gold nanoparticles on VEGF-A-induced cell migration in choroid-retina endothelial cells. Int. J. Mol. Sci. 21. https://doi.org/10.3390/ijms21010109.

Chen, D., Wang, Y., Liu, M., Cheng, J., Liu, Z., Song, Y., Du, J., 2021. Visfatin promotes angiogenesis of RF/6A cells through upregulation of VEGF/VEGFR-2 under high-glucose conditions. Exp. Ther. Med. 21, 389. https://doi.org/10.3892/etm.2021.9820.

Crawford, T.N., Alfaro 3rd, D.V., Kerrison, J.B., Jablon, E.P., 2009. Diabetic retinopathy and angiogenesis. Curr. Diabetes Rev. 5, 8–13. https://doi.org/10.2174/157339909787314149.

Deissler, H.L., Deissler, H., Lang, G.E., 2012. Actions of bevacizumab and ranibizumab on microvascular retinal endothelial cells: similarities and differences. Br. J. Ophthalmol. 96, 1023–1028. https://doi.org/10.1136/bjophthalmol-2012-301677.

Duh, E.J., Sun, J.K., Stitt, A.W., 2017. Diabetic retinopathy: current understanding, mechanisms, and treatment strategies. JCI Insight 2. https://doi.org/10.1172/jci.insight.93751.

Elkjaer, A.S., Lynge, S.K., Grauslund, J., 2020. Evidence and indications for systemic treatment in diabetic retinopathy: a systematic review. Acta Ophthalmol. 98, 329–336. https://doi.org/10.1111/aos.14377.

Gerhardt, H., 2008. VEGF and endothelial guidance in angiogenic sprouting. Organogenesis 4, 241–246. https://doi.org/10.4161/org.4.4.7414.

Goodwin, A.M., 2007. In vitro assays of angiogenesis for assessment of angiogenic and anti-angiogenic agents. Microvasc. Res. 74, 172–183. https://doi.org/10.1016/j.mvr.2007.05.006.

Gudla, S., Tenneti, D., Pande, M., Tipparaju, S.M., 2018. Diabetic Retinopathy: Pathogenesis, Treatment, and Complications. In: Drug Delivery for the Retina and Posterior Segment Disease. Springer International Publishing, Switzerland, pp. 83–94.

Gui, F., You, Z., Fu, S., Wu, H., Zhang, Y., 2020. Endothelial dysfunction in diabetic retinopathy. Front. Endocrinol. 11, 591. https://doi.org/10.3389/fendo.2020.00591.

Han, H., Yang, Y., Wu, Z., Liu, B., Dong, L., Deng, H., Tian, J., Lei, H., 2021. Capilliposide B blocks VEGF-induced angiogenesis in vitro in primary human retinal microvascular endothelial cells. Biomed. Pharmacother. 133, 110999. https://doi.org/10.1016/j.biopha.2020.110999.

Heiss, M., Hellström, M., Kalén, M., May, T., Weber, H., Hecker, M., Augustin, H.G., Korff, T., 2015. Endothelial cell spheroids as a versatile tool to study angiogenesis in vitro. Faseb. J. : Off. Publ. Fed. Am. Soc. Exp. Biol. 29, 3076–3084. https://doi.org/10.1096/fj.14-267633.

Hsu, Y.J., Lin, C.W., Cho, S.L., Yang, W.S., Yang, C.M., Yang, C.H., 2020. Protective effect of fenofibrate on oxidative stress-induced apoptosis in retinal-choroidal vascular endothelial cells: implication for diabetic retinopathy treatment. Antioxidants 9. https://doi.org/10.3390/antiox9080712.

Jin, J., Yuan, F., Shen, M.Q., Feng, Y.F., He, Q.L., 2013. Vascular endothelial growth factor regulates primate choroid-retinal endothelial cell proliferation and tube formation through PI3K/Akt and MEK/ERK dependent signaling. Mol. Cell. Biochem. 381, 267–272. https://doi.org/10.1007/s11010-013-1710-y.

Kern, T.S., Antonetti, D.A., Smith, L.E.H., 2019. Pathophysiology of diabetic retinopathy: contribution and limitations of laboratory research. Ophthalmic Res. 62, 196–202. https://doi.org/10.1159/000500026.

Lai, A.K., Lo, A.C., 2013. Animal models of diabetic retinopathy: summary and comparison. J. Diabetes Res. 2013, 106594. https://doi.org/10.1155/2013/106594.

Lashay, A., Faghihi, H., Mirshahi, A., Khojasteh, H., Khodabande, A., Riazi-Esfahani, H., Amoli, F.A., Pour, E.K., Delrish, E., 2020. Safety of intravitreal injection of stivant, a biosimilar to bevacizumab, in rabbit eyes. J. Ophthalmic Vis. Res. 15, 341–350. https://doi.org/10.18502/jovr.v15i3.7453.

Lazzara, F., Fidilio, A., Platania, C.B.M., Giurdanella, G., Salomone, S., Leggio, G.M., Tarallo, V., Cicatiello, V., De Falco, S., Eandi, C.M., Drago, F., Bucolo, C., 2019. Aflibercept regulates retinal inflammation elicited by high glucose via the PlGF/ERK pathway. Biochem. Pharmacol. 168, 341–351. https://doi.org/10.1016/j.bcp.2019.07.021.

Leung, B.M., Lesher-Perez, S.C., Matsuoka, T., Moraes, C., Takayama, S., 2015. Media additives to promote spheroid circularity and compactness in hanging drop platform. Biomater. Sci. 3, 336–344. https://doi.org/10.1039/c4bm00319e.

Li, M., Wang, S., Wang, S., Zhang, L., Wu, D., Yang, R., Ji, A., Li, Y., Wang, J., 2017. Occludin downregulation in high glucose is regulated by SSTR(2) via the VEGF/NRP1/Akt signaling pathway in RF/6A cells. Exp. Ther. Med. 14, 1732–1738. https://doi.org/10.3892/etm.2017.4651.

Liao, Z.Y., Liang, I.C., Li, H.J., Wu, C.C., Lo, H.M., Chang, D.C., Hung, C.F., 2020. Chrysin inhibits high glucose-induced migration on chorioretinal endothelial cells via VEGF and VEGFR down-regulation. Int. J. Mol. Sci. 21. https://doi.org/10.3390/ijms21155541.

Mehta, G., Hsiao, A.Y., Ingram, M., Luker, G.D., Takayama, S., 2012. Opportunities and challenges for use of tumor spheroids as models to test drug delivery and efficacy. J. Contr. Release : Off. J. Control. Release Soc. 164, 192–204. https://doi.org/10.1016/j.jconrel.2012.04.045.

Moleiro, A.F., Conceição, G., Leite-Moreira, A.F., Rocha-Sousa, A., 2017. A critical analysis of the available in vitro and ex vivo methods to study retinal angiogenesis. J. Ophthalmol. 2017, 3034953. https://doi.org/10.1155/2017/3034953.

Mynampati, B.K., Sambhav, K., Grover, S., Chalam, K.V., 2017. Inhibition of proliferation of retinal vascular endothelial cells more effectively than choroidal vascular endothelial cell proliferation by bevacizumab. Int. J. Ophthalmol. 10, 15–22. https://doi.org/10.18240/ijo.2017.01.03.

Olivares, A.M., Althoff, K., Chen, G.F., Wu, S., Morrisson, M.A., DeAngelis, M.M., Haider, N., 2017. Animal models of diabetic retinopathy. Curr. Diabetes Rep. 17, 93. https://doi.org/10.1007/s11892-017-0913-0.

Park, J., Lee, S., Son, Y., 2016. Effects of two different doses of intravitreal bevacizumab on subfoveal choroidal thickness and retinal vessel diameter in branch retinal vein occlusion. Int. J. Ophthalmol. 9, 999–1005. https://doi.org/10.18240/ijo.2016.07.11.

Pereira, P.M.R., Berisha, N., Bhupathiraju, N., Fernandes, R., Tomé, J.P.C., Drain, C.M., 2017. Cancer cell spheroids are a better screen for the photodynamic efficiency of glycosylated photosensitizers. PLoS One 12, e0177737. https://doi.org/10.1371/journal.pone.0177737.

Peters, S., Julien, S., Heiduschka, P., Grisanti, S., Ziemssen, F., Adler, M., Schraermeyer, U., Bartz-Schmidt, K.U., 2007. Antipermeability and antiproliferative effects of standard and frozen bevacizumab on choroidal endothelial cells. Br. J. Ophthalmol. 91, 827–831. https://doi.org/10.1136/bjo.2006.109702.

Rezzola, S., Belleri, M., Gariano, G., Ribatti, D., Costagliola, C., Semeraro, F., Presta, M., 2014. In vitro and ex vivo retina angiogenesis assays. Angiogenesis 17, 429–442. https://doi.org/10.1007/s10456-013-9398-x.

Rezzola, S., Nawaz, I.M., Cancarini, A., Ravelli, C., Calza, S., Semeraro, F., Presta, M., 2017. 3D endothelial cell spheroid/human vitreous humor assay for the characterization of anti-angiogenic inhibitors for the treatment of proliferative diabetic retinopathy. Angiogenesis 20, 629–640. https://doi.org/10.1007/s10456-017-9575-4.

Rusovici, R., Sakhalkar, M., Chalam, K.V., 2011. Evaluation of cytotoxicity of bevacizumab on VEGF-enriched corneal endothelial cells. Mol. Vis. 17, 3339–3346.

Rusovici, R., Patel, C.J., Chalam, K.V., 2013. Bevacizumab inhibits proliferation of choroidal endothelial cells by regulation of the cell cycle. Clin. Ophthalmol. 7, 321–327. https://doi.org/10.2147/opth.S41556.

Saeedi, P., Petersohn, I., Salpea, P., Malanda, B., Karuranga, S., Unwin, N., Colagiuri, S., Guariguata, L., Motala, A.A., Ogurtsova, K., Shaw, J.E., Bright, D., Williams, R., 2019. Global and regional diabetes prevalence estimates for 2019 and projections for 2030 and 2045: results from the international diabetes federation diabetes atlas. Diabetes Res. Clin. Pract. 157, 107843. https://doi.org/10.1016/j.diabres.2019.107843.

Sarkar, A., Dyawanapelly, S., 2021. Nanodiagnostics and Nanotherapeutics for age-related macular degeneration. J. Contr. Release : Off. J. Control. Release Soc. 329, 1262–1282. https://doi.org/10.1016/j.jconrel.2020.10.054.

Semeraro, F., Cancarini, A., dell'Omo, R., Rezzola, S., Romano, M.R., Costagliola, C., 2015. Diabetic retinopathy: vascular and inflammatory disease. J. Diabetes Res., 582060 https://doi.org/10.1155/2015/582060.

Spitzer, M.S., Wallenfels-Thilo, B., Sierra, A., Yoeruek, E., Peters, S., Henke-Fahle, S., Bartz-Schmidt, K.U., Szurman, P., 2006. Antiproliferative and cytotoxic properties of bevacizumab on different ocular cells. Br. J. Ophthalmol. 90, 1316–1321. https://doi.org/10.1136/bjo.2006.095190.

Stefanini, M.O., Wu, F.T., Mac Gabhann, F., Popel, A.S., 2009. The presence of VEGF receptors on the luminal surface of endothelial cells affects VEGF distribution and VEGF signaling. PLoS Comput. Biol. 5, e1000622. https://doi.org/10.1371/journal.pcbi.1000622.

Tetzlaff, F., Fischer, A., 2018. Human endothelial cell spheroid-based sprouting angiogenesis assay in collagen. Bio-protocol 8, e2995. https://doi.org/10.21769/BioProtoc.2995.

Van Norman, G.A., 2019. Limitations of animal studies for predicting toxicity in clinical trials: is it time to rethink our current approach? JACC Basic Transl. Sci. 4, 845–854. https://doi.org/10.1016/j.jacbts.2019.10.008.

Wang, W., Lo, A.C.Y., 2018. Diabetic retinopathy: pathophysiology and treatments. Int. J. Mol. Sci. 19. https://doi.org/10.3390/ijms19061816.

Wang, C., Lin, Y., Fu, Y., Zhang, D., Xin, Y., 2020. MiR-221-3p regulates the microvascular dysfunction in diabetic retinopathy by targeting TIMP3. Pflueg. Arch. Eur. J. Physiol. 472, 1607–1618. https://doi.org/10.1007/s00424-020-02432-y.

Whitehead, M., Wickremasinghe, S., Osborne, A., Van Wijngaarden, P., Martin, K.R., 2018. Diabetic retinopathy: a complex pathophysiology requiring novel therapeutic strategies. Expet Opin. Biol. Ther. 18, 1257–1270. https://doi.org/10.1080/14712598.2018.1545836.

Wong, T.Y., Sabanayagam, C., 2020. Strategies to tackle the global burden of diabetic retinopathy: from epidemiology to artificial intelligence. Ophthalmologica 243, 9–20. https://doi.org/10.1159/000502387.

Xu, Y., Zhao, H., Zheng, Y., Gu, Q., Ma, J., Xu, X., 2010. A novel antiangiogenic peptide derived from hepatocyte growth factor inhibits neovascularization in vitro and in vivo. Mol. Vis. 16, 1982–1995.

Yu, Z., Zhang, T., Gong, C., Sheng, Y., Lu, B., Zhou, L., Ji, L., Wang, Z., 2016. Erianin inhibits high glucose-induced retinal angiogenesis via blocking ERK1/2-regulated HIF-1α-VEGF/VEGFR2 signaling pathway. Sci. Rep. 6, 34306. https://doi.org/10.1038/srep34306.

Zucchelli, E., Majid, Q.A., Foldes, G., 2019. New artery of knowledge: 3D models of angiogenesis. Vasc. Biol. 1, H135–h143. https://doi.org/10.1530/vb-19-0026.